Bulgarian Chemical Communications, Volume 53, Issue 2 (pp. 196 - 210) 2021 *DOI: 10.34049/bcc.53.2.5329*

Theoretical investigation of inclusion complex of 2-methyl mercapto phenothiazine with hydroxy propyl β-cyclodextrin by DFT approaches

Y. Mezari[1], L. Nouar[2]*, F. Madi[2], A. Guendouzi[3,4], I. Djellala[2], I. Lafifi[2], R. Merdes[1], A. Bouhadiba[5], B. Houari[3]

[1]*Laboratory of Applied Chemistry, Department of Material Sciences, Faculty of Mathematical, Informatics and Material Sciences, University of 8 Mai 1945, Guelma, Algeria*
[2]*Laboratory of Computational Chemistry and Nanostructures, Department of Material Sciences, Faculty of Mathematical, Informatics and Material Sciences, University of 8 Mai 1945, Guelma, Algeria*
[3] *Laboratory of Chemistry, Synthesis, Properties and Applications, Department of Chemistry, Faculty of Sciences, University of Saïda, Algeria*
[4] *Laboratory of Applied Thermodynamics and Molecular Modeling, University Abu Bekr Belkaïd of Tlemcen, Algeria*
[5]*Laboratory of Computational Chemistry and Nanostructures, University of Skikda, Algeria*

Received: September 24, 2020; Revised: February 02, 2021

The supramolecular host-guest complexation of 2-methyl mercapto phenothiazine with hydroxy propyl β-cyclodextrin is computationally investigated employing B97-D3 and BP86-D3 levels of theory with 6-31G(d,p) basis set in gas and aqueous phases. The computed binding and interaction energies values reflect the stability of the studied inclusion complexes. EDA, TD-DFT, NBO, QTAIM and NCI analyses were done to give more information about the nature of intermolecular interaction between 2-methyl mercapto phenothiazine and hydroxy propyl β-cyclodextrin. The results show that the inclusion complexes are stabilized by hydrogen bonding and van der Waals interactions. Finally, our theoretical ^{1}H NMR chemical shift results are in good agreement with the experimental data.

Keywords*:* Inclusion complex, interaction energies, Fukui function, electronic transitions, non-covalent interactions.

INTRODUCTION

In recent years, quantum chemical approaches have become a valuable tool to understand the nature of interactions in supramolecular systems. These interactions play important roles in molecular properties. A deep understanding of intermolecular non-covalent interactions has been one of the main tasks in theoretical chemistry. Several parameters contribute to quantify the nature of non-covalent intermolecular interactions in supramolecular systems [1]. These parameters can be divided in four categories: energy decomposition analysis (EDA), which provides quantitative analysis for intermolecular interactions *via* dividing total interaction energy into several physically meaningful energy quantities, atoms in molecules (AIM) [2] to inspect the nature of weak interactions in supramolecular complexes; non-covalent interactions (NCI) analysis has been widely used to visualize the interaction in the supramolecular host–guest system [3] and NBO analysis, in which intermolecular interaction energy is estimated by charge transfers between donating and accepting orbitals [4].

Phenothiazines are organic compounds related to the thiazine class of heterocyclic compounds. They have antipsychotic, antiemetic, anthelmintic, antibacterial, antifungal, insecticidal and anticancer properties [5]. 2-Methyl mercapto phenothiazine (2MMPT) (10-[2-(1-methyl-2-piperidyl)ethyl]-2-(methylthio)-10H-phenothiazine thioridazine) (Fig. 1) is one of the phenothiazine substituents showing strong antiproliferative activity against various breast, ovarian, lungs, and melanoma cell lines [6]. However, phenothiazine derivatives have a low solubility in water [7] possibly limiting its range of applications. Therefore, complexation with cyclodextrin is a significant method to increase the solubility, bioavailability and biological activities of phenothiazine drugs.

Cyclodextrins (CDs), are cyclic oligomers of α-D-glucose units connected through glycosidic α-1,4 bonds, which can form inclusion complexes with a variety of organic compounds [8]. The most widely used CDs are α-, β- and γ-CDs. Compared to α- and γ-cyclodextrins, β-cyclodextrin (β-CD) is most useful. However, the solubility of β-CD is relatively low [9]. Hydroxy propyl β-cyclodextrin (HPβ-CD) is a substitute for β-CD and has higher water solubility than β-CD. Hydroxy propyl β-cyclodextrin (Fig. 1) has attracted growing research interest owing to its low toxicity, satisfactory inclusion ability and capacity to improve the physico-chemical properties and the solubility of poorly water-soluble drugs [10].

* To whom all correspondence should be sent:
E-mail: leilanoua@yahoo.fr, nouar.leila@univ-guelma.dz

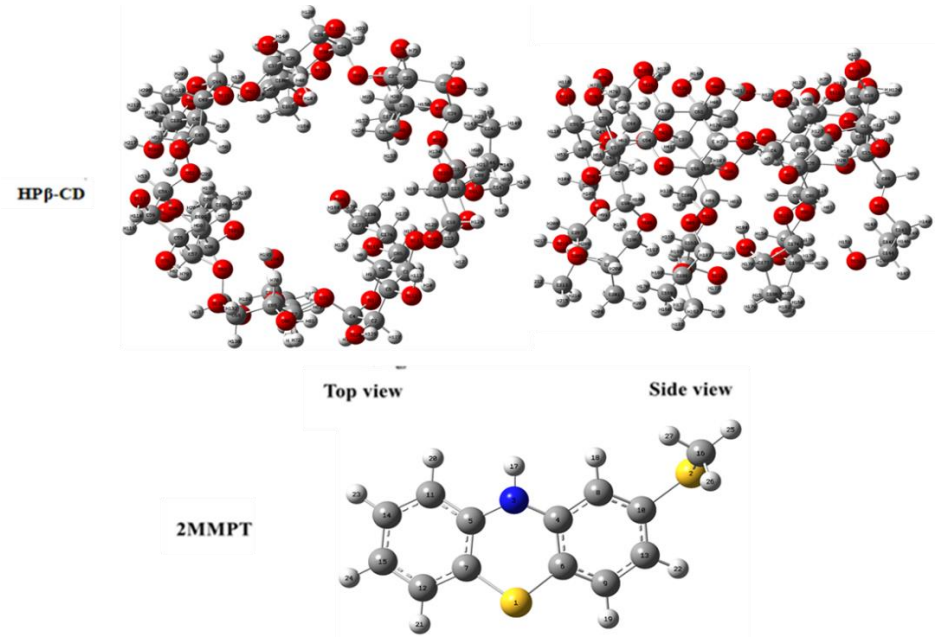

Fig. 1. Molecular structures and atom numbering for HPβ-CD and 2MMPT.

The complexation involving 2MMPT and HPβ-CD has been studied experimentally for improving solubility and bioavailability of the active principle [11]. However, in the latter work, no information about the nature of intermolecular non-covalent interactions between host and guest of the complex was provided.

The aim of this work is to study the nature of non-covalent intermolecular interactions, especially hydrogen bond interaction between 2MMPT and HPβ-CD during inclusion complex formation.

Therefore, the present work is organized as follows: Firstly, in computational details we describe the formation of the complex between HPβ-CD and 2MMPT, using PM3 semi-empirical method to localize the minimum energy structures. Secondly, the most stable complexes, found by PM3 calculations, were re-optimized by the DFT-D3 method. Thirdly, the analysis results of the intermolecular non-covalent interactions are discussed.

Computational details

Geometry optimizations were performed by PM3 and DFT using the dispersion corrected with the Grimme's D3 correction [12-14]. For the complexation process, we followed the method described in our previous studies [15, 16]. The oxygen atoms of glycosidic bond links of HPβ-CD were placed onto the (XY) plane. Their center was set as the center of the coordination system. The secondary (OH) groups of the HPβ-CD were positioned pointing toward the Z-axis in the positive direction. The 2MMPT molecule was initially oriented along the Z-axis. We considered in this process two possible inclusion models with HPβ-CD. The model in which the phenyl ring of 2MMPT points toward the secondary hydroxyl of HPβ-CD was called the "C1 complex", the other model in which 2MMPT penetrates into the cavity of HPβ-CD from its wide side by the SCH_3 group was called the "C2 complex". The inclusion models can be seen in Fig. 2. The relative position between the host and the guest was determined by the Z-coordinate of the labelled nitrogen atom (N220) of the guest (Fig. 2). Then, the guest was moved into the HPβ-CD cavity along the Z-axis from −6 to +6 Å with 1 Å step. The generated structures at each step were optimized by the PM3 method without imposing any symmetrical restrictions. On the other hand, the generated structures at each step were analyzed by EDA analysis. After that, the obtained global minimas were fully re-optimized within any restriction at B97-D3 and BP86-D3 levels of theory with 6-31G (d, p) basis set in gas and aqueous phases. The solvent effects in water (ε=78.5) were evaluated by a conductor polarizable continuum model (CPCM). Harmonic vibrational frequencies were computed for the minimum energy geometries to verify them to be at the minimum on the potential surface. Statistical thermodynamic calculations were carried out at 1 atm and 298.15 K in gas and aqueous phases. The gauge-independent atomic orbital (GIAO) method [17] was used to compute ^{1}H NMR chemical shifts of free and complexed 2MMPT.

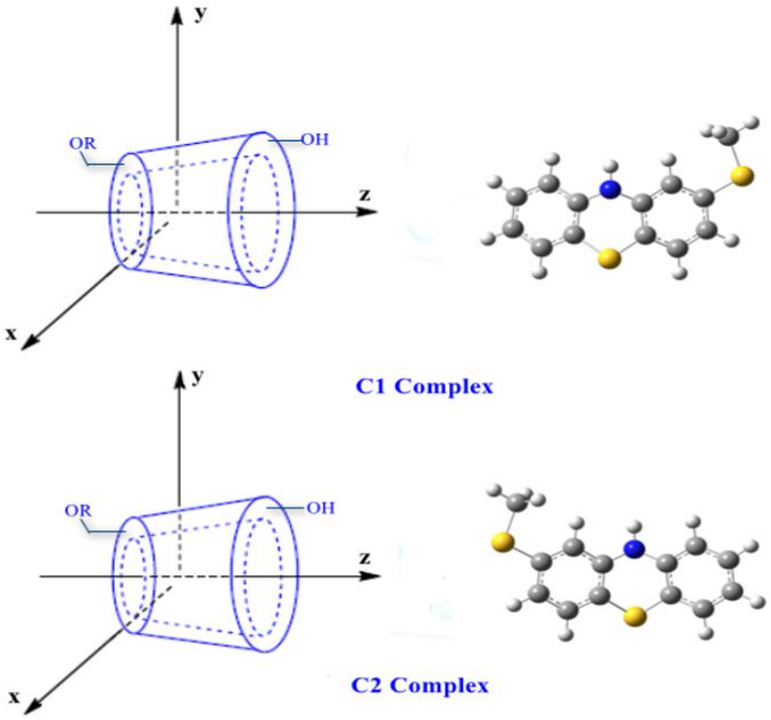

Fig. 2. Proposed structures of 2MMPT @ HPβ-CD inclusion complexes.

Electronic transitions by time-dependent density functional theory (TD-DFT) and the frequency shift in the calculated vibrational spectra were explained. Finally, to identify the nature of non-covalent intermolecular interactions between host and guest on the optimized structures with the lowest energynin aqueous phase at BP86-D3/6-31G(d,p) level of theory, we investigated the natural bond orbital (NBO), atoms-in-molecules (AIM) and the non-covalent interactions in the complexes using the non-covalent interaction-reduced density gradient (NCI-RDG) analyses. Geometry optimizations and NBO calculations were carried out using the Gaussian 09 package [18]. QTAIM and NCI-RDG analyses were envisaged using the Multiwfn program [19] and visualized by the VMD program [20]. EDA analysis was performed using the ADF package [21].

RESULTS AND DISCUSSION

Energies, geometries and thermodynamic parameters

The PM3 calculation was used in this study to localize global minima through Z-axis for C1 and C2 complexes by controlling binding energy during the inclusion process of 2MMPT into HPβ-CD cavity.

To evaluate the stability of the obtained complexes, we calculated binding, interaction and strain energies using the following eqs.:

$$\Delta E_{binding} = E_{binding} - \left(E_{HP\beta-CD} + E_{2MMPT}\right) \quad (1)$$

where $E_{binding}$, $E_{HP\beta\text{-}CD}$ and E_{2MMPT} represent the total energy of the complex, the free optimized HPβ-CD and the free optimized 2MMPT energy, respectively. The binding energy corresponds to the energy change accompanying the inclusion of 2MMPT in HPβ-CD:

$$\Delta E_{interaction} = E_{complex} - \left(E^{sp}_{HP\beta-CD} + E^{sp}_{2MMPT}\right) \quad (2)$$

where $E_{complex}$, $E^{sp}{}_{HP\beta\text{-}CD}$and $E^{sp}{}_{2MMPT}$ are the total energy and the single point energy of the HPβ-CD and 2MMPT molecules in the optimized complexes, respectively.

$$\Delta E_{strain} = (E^{SP}_{component} - E^{free}_{component}) \quad (3)$$

where $E^{SP}{}_{component}$ is the single point energy of the component (HPβ-CD or 2MMPT) in the optimized complex and $E_{component}$ is the energy when it is optimized in free form.

The variation of the binding energy for both complexes is illustrated in Fig. 3. As it can be seen, all values of binding energy are negative, which indicates that the inclusion process of the 2MMPT in the HPβ-CD is thermodynamically favorable. The lowest binding energies were obtained at Z= -3 Å and Z = -4 Å for C1 and C2 complexes, respectively.

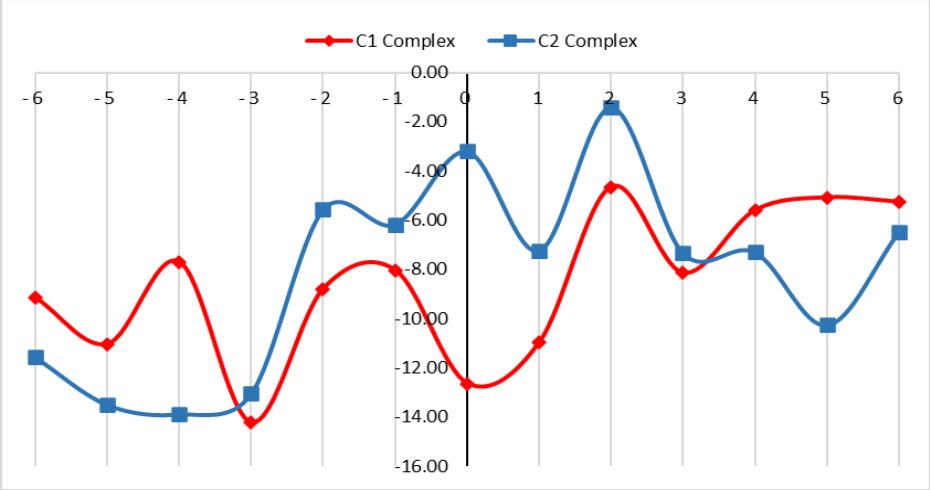

Fig. 3. Variation of the binding energy for both complexes at different positions, PM3 calculations.

The calculated binding, interaction and strain energies for the most stable structures in gas and in aqueous phases are mentioned in Table 1. We noticed that the binding energy in gas phase is in favor of the C1 complex by 1.78 and 4.28 kcal/mol, respectively, by the B97-D3/6-31G(d,p) and BP86-D3/6-31G(d,p) methods. In aqueous phase, the results of calculations listed in Table 1 confirm those obtained in gas phase and the binding energy difference in aqueous phase for B97-D3/6-31G(d, p) and BP86-D3/6-31G(d,p) calculations between the two complexes is 4.11 and 8.62 kcal/mol, respectively, in favor of the C1 complex.These energies are higher in gas phase than in aqueous phase, because the water molecules can weaken the intermolecular interactions between the host and guest molecules.

In addition, interaction energy is an important parameter also measuring the stability of inclusion complexes; it is found more negative for the two complexes in both gas and aqueous phases with BP86-D3/6-31G (d, p) calculations.

Binding and interaction energies in gas and in aqueous phases with two functionals follow the order B97-D3/6-31G (d,p) > BP86-D3/6-31G(d,p). BP86-D3/6-31G (d,p) gave the most negative values of binding and interaction energies for studying our systems.

The distortion in the geometry of the 2MMPT and HPβ-CD molecules in gas and in aqueous phases is reflected in the calculated strain energy (ΔE_{strain}). The ΔE_{strain} values for the HPβ-CD are larger than that of 2MMPT in the two complexes. The great deformation of HPβ-CD structure has an important role in increasing the intermolecular interaction of the complexes. From these results it can be concluded that the distortion in the geometry of the host seems to be one of the driving factors leading to the formation of stable inclusion complexes. In Fig. 4, we illustrated the geometrical structures of the most stable C1 and C2 complexes obtained from B97-D3/6-31G (d,p) and BP86-D3/6-31G(d,p) calculations in both phases. We noticed that the 2MMPT molecule is totally embedded in the HPβ-CD cavity. Hydrogen bonds established between the host and guest molecules in the C1 complex are stronger than those in the C2 complex (see Fig. 4 and Table 1S). In this sense, the hydrogen bonds can be considered the driving forces responsible for the difference in binding energies between the two complexes. The structure of the C1 complex agrees well with experimental results, which indicated that the aromatic part of 2MMPT was included into the cavity of HPβ-CD from its wide side and formed an inclusion complex [11].

From the vibrational frequency computations and statistical thermodynamics, the standard thermodynamic parameters, *viz*., enthalpy (ΔH°) and free energy (ΔG°) of the inclusion complexes in gas and in aqueous phases were calculated and are summarized in Table 1. Negative values for ΔH° and ΔG° indicate that the formation of the complexes is an exothermic and spontaneous process. This result is in good agreement with experimental data [11]. However, ΔH° and ΔG° values for the C1 complex obtained from B97-D3/6-31G(d,p) and BP86-D3/6-31G(d,p) functional in gas and in aqueous phases are lower than for the C2 complex, indicating that formation of this complex is a weak exothermic process.

Table 1. Energies (kcal/mol) and thermodynamic parameters for both complexes in gas and in aqueous phases.

Methods	B97-D3/6-31G(d, p)		BP86-D3/6-31G(d, p)	
	C1	C2	C1	C2
In gas phase				
$\Delta E_{Binding}$	-42.87	-41.09	-47.46	-43.18
$\Delta E_{Interaction}$	-56.22	-53.06	-63.32	-63.47
$\Delta E_{Strain\ (HP\beta CD)}$	10.26	9.87	11.72	16.98
$\Delta E_{Strain\ (2MMPT)}$	3.11	2.10	4.14	3.31
$\Delta H°(kcal.mol^{-1})$	-39.78	-32.14	-45.22	-40.79
$\Delta G°(kcal.mol^{-1})$	-29.69	-16.02	-28.14	-22.94
In aqueous phase				
$\Delta E_{Binding}$	-38.27	-34.16	-50.87	-42.25
$\Delta E_{Interaction}$	-47.74	-41.46	-58.94	-54.70
$\Delta E_{Strain\ (HP\beta CD)}$	6.37	6.51	4.41	9.72
$\Delta E_{Strain\ (2MMPT)}$	3.10	0.79	3.66	2.74
$\Delta H°(kcal.mol^{-1})$	-35.85	-33.63	-47.99	-39.50
$\Delta G°(kcal.mol^{-1})$	-19.19	-17.08	-29.49	-22.06

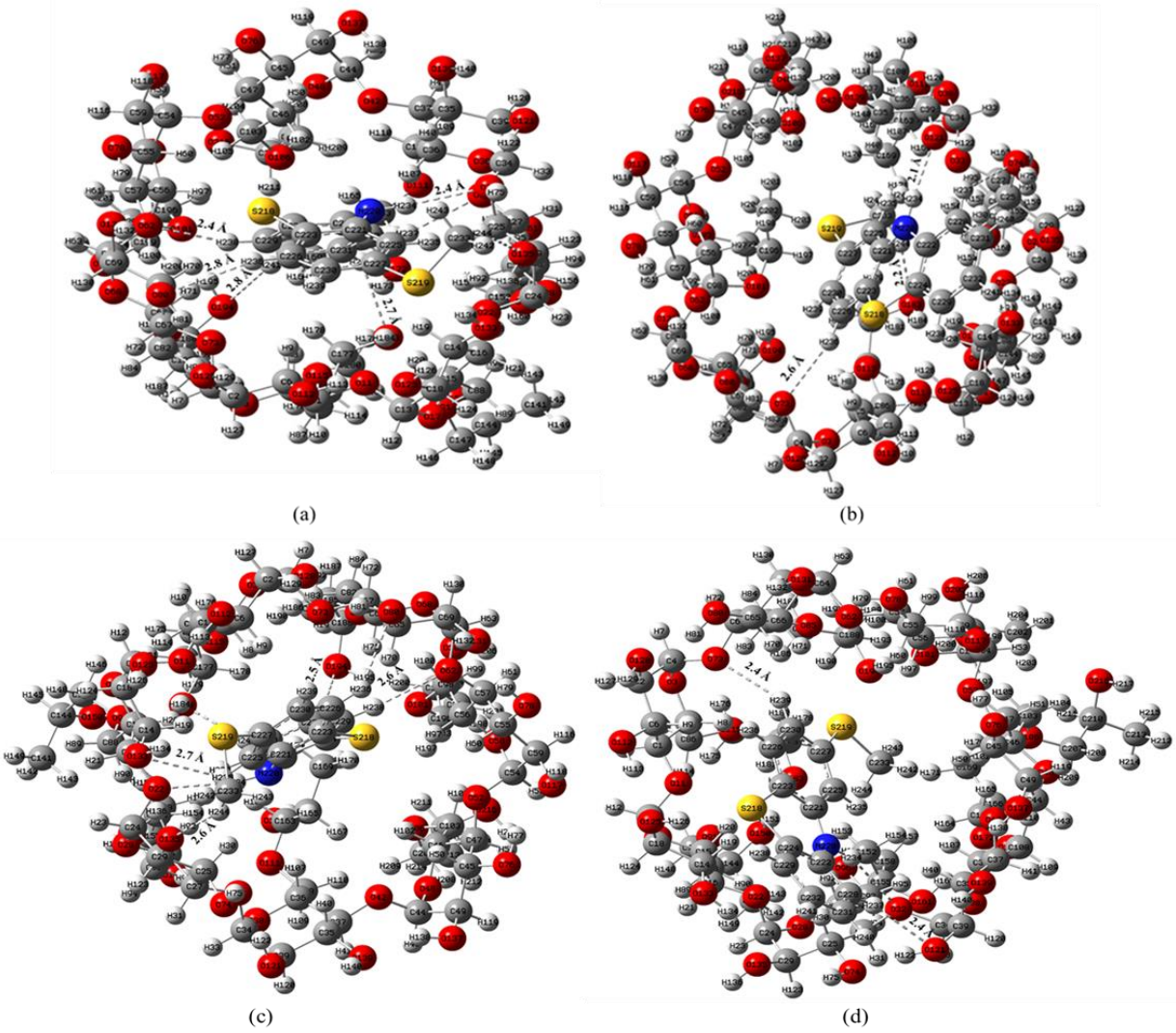

In gas phase

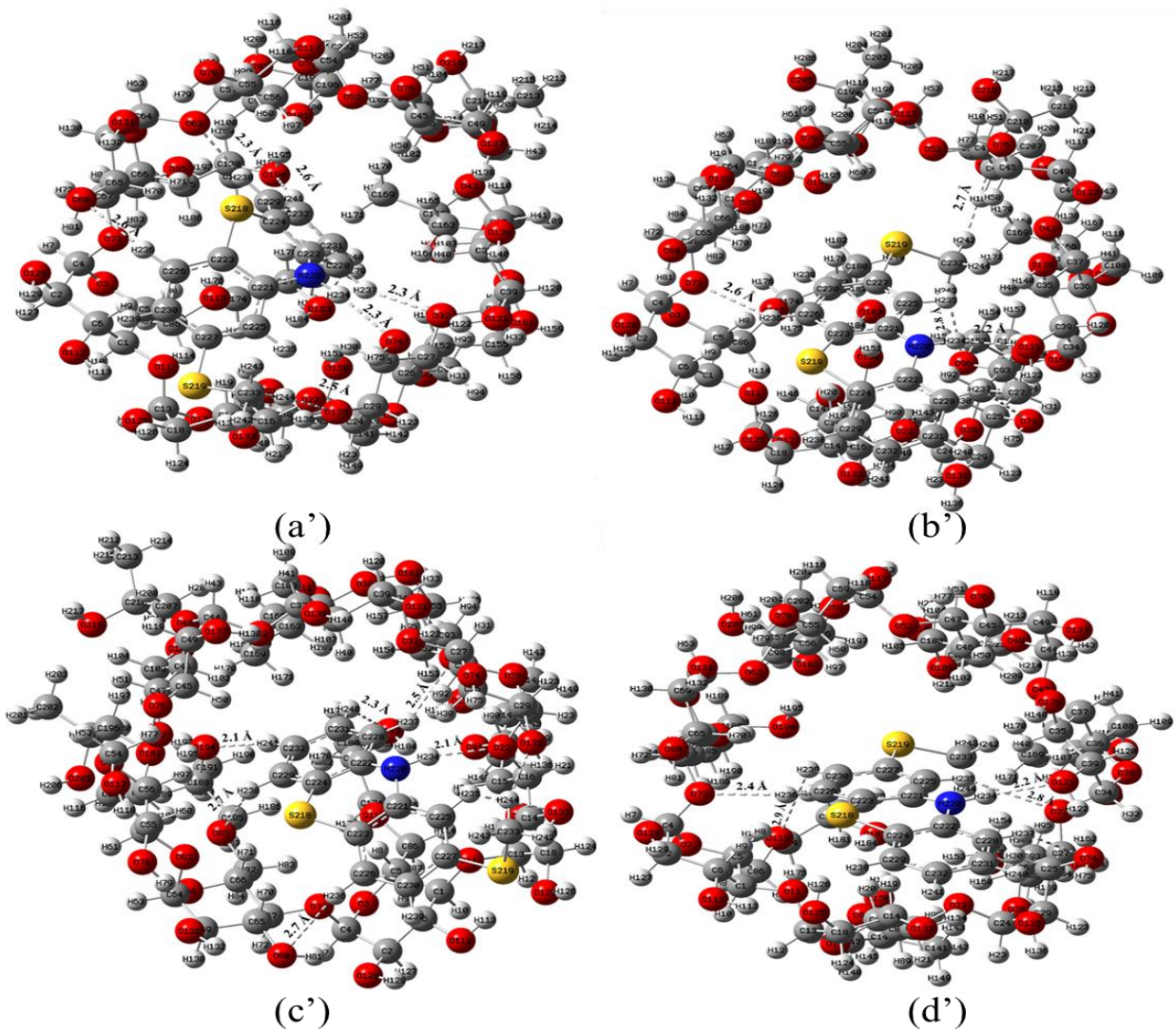

In aqueous phase

Fig.4. Optimized structures of inclusion complexes obtained from B97-D3/6-31G(d,p) (a, b, a', b') and BP86-D3/6-31G(d,p) (c, d, c', d') calculations. (a, b, c, d) in gas and in aqueous phases (a', b', c', d'), respectively, for C1 and C2 complexes.

Local reactivity descriptors

The local reactivity was analyzed with the aid of the Fukui indices, the condensed Fukui functions [22-24] for the reactive sites of electrophilic and nucleophilic attack on the molecules, which can be expressed as:

For nucleophilic attack:

$$f_k^+ = [q_k (N + 1) - q_k (N)] \quad (4)$$

For electrophilic attack:

$$f_k^- = [q_k (N) - q_k (N - 1)] \quad (5)$$

For radical attack:

$$f_k^0 = [q_k (N + 1) - q_k (N - 1)] / 2 \quad (6)$$

where +, -, 0 signs refer to nucleophilic, electrophilic and radical attack, respectively.

The Fukui index for electrophilic attack (f_k^-) represents the nucleophilic site of the species and the Fukui index for nucleophilic attack (f_k^+) represents the electrophilic site of the species [25]. Condensed Fukui functions (f_k^+, f_k^-) associated with the nucleophilic and electrophilic attacks, using natural population analysis (NPA) of 2MMPT (Scheme 1S) before and after complexation in aqueous phase, are reported in Table 2S. To compare between the possible sites for nucleophilic and electrophilic attacks on any atom, we calculated (Δf_k) which corresponds to the difference ($f_k^+ - f_k^-$). If $\Delta f_k < 0$, then the site is favorable for an electrophilic attack, whereas if $\Delta f_k > 0$, then the site is favorable for a nucleophilic attack. As can be observed, for an isolated 2MMPT molecule S1, S2 and N3 are the most nucleophilic sites, whereas C13 and C14 are the electrophilic sites. After complexation, the values of the dual descriptor are also changed

comparatively to the free 2MMPT. S1, S2 and N3 are the most nucleophilic sites with a slight decrease in values of $f_{(k)}^{-}$. C7 and C10 become favorable electrophilic sites. Condensed Fukui functions in the gas phase are illustrated in Table 3S. As can be seen from Table 3S, nucleophilic and electrophilic attacks in gas phase are the same to those obtained in the aqueous phase with difference in values of the Fukui indices. The plots of the Fukui indices for isolated 2MMPT and the two complexes in gas and in aqueous phases are presented in Fig. 5.

Electronic transitions and UV–Vis spectra

The electronic transitions of the two complexes were calculated using the time-dependent density functional theory (TD-DFT) at BP86-D3/6-31G (d, p) level using ground-state geometries in aqueous phase. The calculated excitation energies, oscillator strength (*f*) and wavelength (λ) and configurations of excitations are given in Table 4S. For the C1 complex, TD-DFT calculations predict two transitions in the UV–Vis region. A strong transition is observed at 2.9414 eV (421.51 nm) with an oscillator strength f = 0.0078. This peak is due to electronic transition from HOMO-1→LUMO. For the C2 complex three transitions are observed, a strong one at 410.59 nm with vertical transitions and oscillator strength equal to 3.0196 and 0.0046 eV, respectively. This band is obtained between HOMO→LUMO. A careful inspection of molecular plots of encapsulated complexes (Fig. 6) shows that in the C1 complex, the HOMO-1 is localized on the HPβ-CD molecule and LUMO is localized on 2MMPT revealing a high charge transfer in the complex. In the C2 complex, the HOMO and LUMO orbitals are localized on the 2MMPT molecule, which shows that this excitation arises from a local excited state.

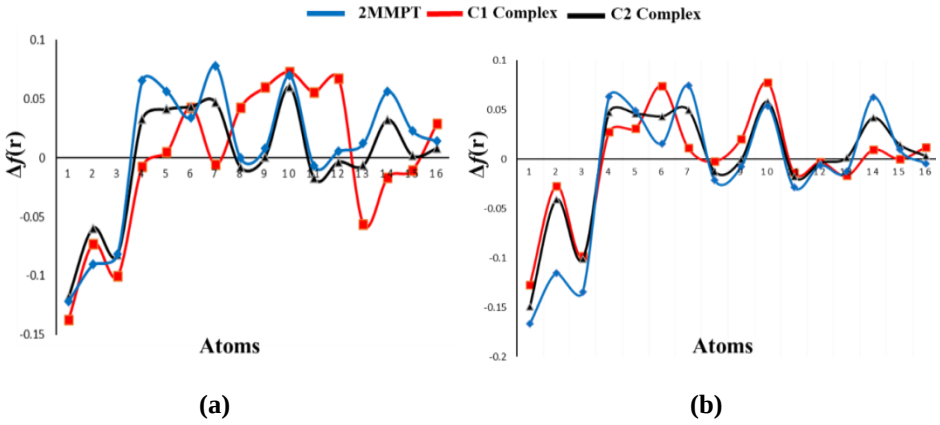

Fig. 5. Plots of the Fukui indices for the isolated 2MMPT and the two complexes in gas (a) and in aqueous (b) phase.

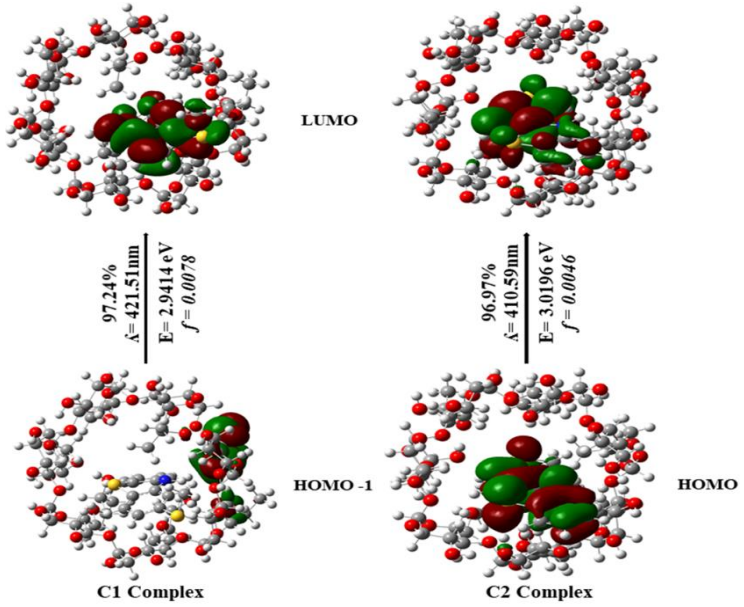

Fig. 6. Plots of molecular orbitals for vertical excitation energies (E, eV), oscillator strengths (f) and wavelength (λ) for C1 and C2 complexes calculated at BP86-D3/6-31G (d,p) in aqueous phase.

NMR spectral studies

Based on BP86-D3/6-31G (d,p) optimized geometries, the gauge-including atomic orbital (GIAO) method was applied for ^{1}H NMR calculations by employing the density functional theory B3LYP at 6-31G (d,p) basis set by using corresponding TMS shielding calculated at the same theoretical level as the reference. The calculated proton chemical shifts of isolated and complexed 2MMPT (Scheme 1S) are recorded in Table 2. We noticed a significant change in chemical shift values of 2MMPT in the two complexes. This significant chemical shift change confirmed the encapsulation of 2MMPT into the hydrophobic cavity of HPβ-CD and the formation of an inclusion complex between 2MMPT and HPβ-CD. On the other hand, the computed shielding obtained for the optimized structures from the GIAO theory analysis for C1 and C2 complexes plotted as a function of the experimental chemical shift parameters [11] displayed in Fig. 7 turns out to be linear. The linear regression equation is expressed by the following regression expressions:

$\delta_{Calculated} = 1.0704\ \delta_{experimental} - 0.5988$,

with correlation coefficient $R^2 = 0.96$ for the C1 complex and

$\delta_{Calculated} = 0.8106\ \delta_{experimental} + 0.7669$,

with $R^2 = 0.90$ for the C2 complex.

The best linear correlation between calculated and experimental chemical shift is observed in the C1 complex; however, our theoretical ^{1}H NMR chemical shift results for the C1 complex are in good agreement with the experimental data [11].

Table 2. ^{1}H NMR chemical shift (δ, ppm) in D_2O obtained by the GIAO approach for free and complexed 2MMPT as calculated at B3LYP-D3/6-31G(d,p) level of theory and chemical shift displacement Δδ after complexation.

$\Delta\delta = \delta_{2MMPT\ in\ complex} - \delta_{2MMPT\ free}$

Proton	2MMPT calculated	2MMP Texp	C 1 complex	C 2 complex	2MMPT@ HPβ-CDexp	$\Delta\delta_{C\,1}$ complex	$\Delta\delta_{C2}$ complex	$\Delta\delta_{exp}$
H_a	5.420	5.798	5.353	5.248	5.802	0.067	0.173	0.004
H_b	6.031	7.254	6.507	5.822	7.262	0.477	0.208	0.008
H_c	6.675	7.001	6.949	6.425	7.011	0.274	0.25	0.01
H_d	6.712	6.894	6.709	6.371	6.904	0.003	0.340	0.01
H_e	6.893	6.732	6.811	6.550	6.743	0.082	0.343	0.011
H_f	6.911	6.542	6.923	6.584	6.542	0.012	0.326	0
Hg	7.014	6.840	6.912	6.725	6.847	0.102	0.289	0.007
H_h	6.464	6.462	6.463	5.912	6.481	0.001	0.552	0.019
H_i	2.402	2.423	1.957	2.681	2.436	0.451	0.279	0.013
H_j	2.137	/	2.452	1.968	/	0.315	0.169	/
H_k	2.137	/	2.573	2.335	/	0.436	0.198	/

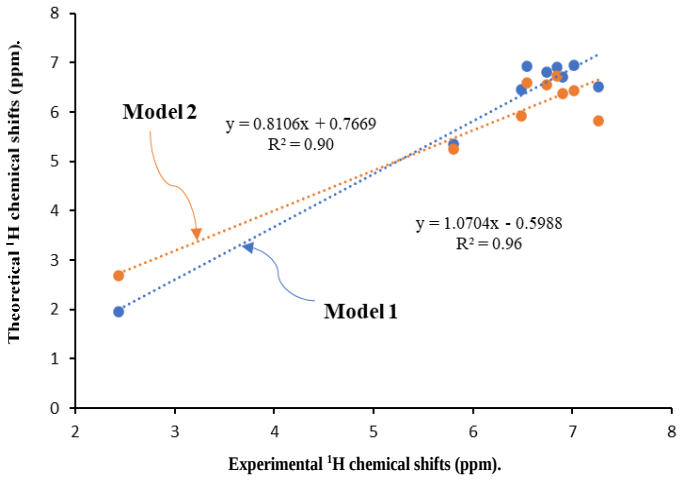

Fig. 7. Correlation between calculated and experimental chemical shifts.

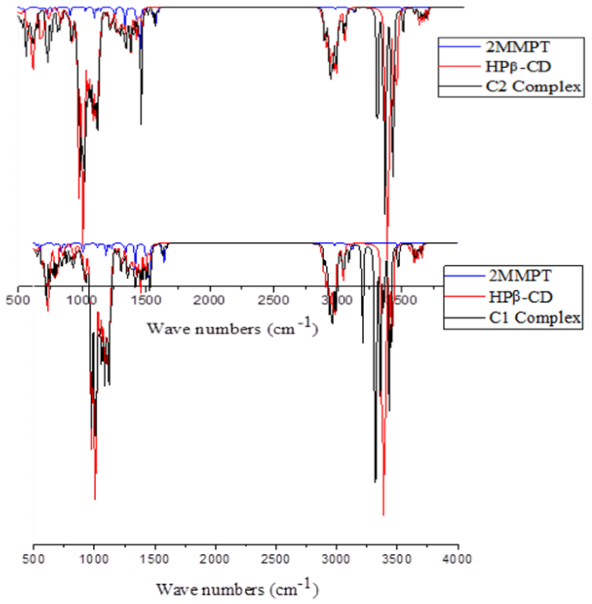

Fig. 8. FT-IR spectra of 2MMPT (in blue), HPβ-CD (in red) and 2MMPT@HPβ-CD (in black) inclusion complexes.

Vibrational spectra

Vibrational frequencies are useful for probing interatomic interactions between host and guest in the two complexes. The infrared spectra of HPβ-CD, 2MMPT, C1 and C2 inclusion complexes are shown in Fig. 8. BP86-D3/6-31G (d,p) computed spectra of the complexes (depicted in black) are compared with the individual HPβ-CD (red) and 2MMPT (blue) spectra. The theoretical and experimental frequencies are presented in Table 5S. As shown in Table 5S and in Fig. 8, for HPβ-CD, peaks were observed at 3398 cm^{-1}, 2950 cm^{-1}, 921 cm^{-1} and 1120 cm^{-1}, respectively, for O-H stretching, C-H stretching, C-H bending and C-O stretching vibrations. Upon complexation with 2MMPT, these vibrational frequencies reveal up-shift tendencies. In the case of 2MMPT, the bands resulting from inclusion complexes are shifted or their intensities are changed. The highly intense band at 3500 cm^{-1} assigned to the N-H stretching shows downshift in the two complexes. The C-H stretching and C-S stretching vibrations show down-shift. The C=C stretching, C-C stretching and C-H bending vibrations show up-shift in their vibrational frequencies. N-H bending shows up-shift for the C1 complex and down-shift for the C2 complex. In addition, C-N stretching and C-S-CH_3 stretching vibrations reveal a shift in their frequencies. These results indicated that the 2MMPT was included into the cavity of HPβ-CD and formed an inclusion complex. The selected calculated vibrational frequencies in the C1 and C2 complexes given in Table 5S are generally in consonance with these obtained in experimental data [11].

Recently, Lane *et al.* [26] demonstrated that the analysis of the kinetic energy density G(r) features at the hydrogen bond critical points could be correlated to spectroscopic features of the X-H stretching involved in hydrogen bond formation. With this view the calculated kinetic energy density G(r) was plotted as a function of the frequency shift in Fig. 2S. The plot reveals an excellent linear correlation.

Natural bond orbital analysis

The natural bonding orbital (NBO) analysis provides an efficient method for studying intra- and intermolecular bonding and for investigating charge transfer or conjugative interaction in molecular systems [27]. Also it can be used to estimate delocalization of the electron density between occupied Lewis-type orbitals and unoccupied non-Lewis NBOs, which corresponds to a stabilizing donor–acceptor interaction [28]. In the NBO analysis the stabilization or second-order perturbation energy $E^{(2)}$ is a value of energy by which the whole of the molecular systems is stabilized through charge transfer from donor to acceptor groups, and the large $E^{(2)}$ value shows the intense interaction between electron donors and electron acceptors and the greater extent of conjugation of the whole system [29]. This second-order perturbation energy $E^{(2)}$ is defined by:

$$E^{(2)} = qi\frac{F(i,j)}{\varepsilon j - \varepsilon i} \quad (7)$$

where qi is the donor occupancy, εi and εj are diagonal elements (orbital energies), and F(i,j) are off-diagonal elements of NBO Fock matrix. Natural bond orbital (NBO) donors and acceptors and their second-order perturbation energy values $E^{(2)}$ in both gas and aqueous phases for C1 and C2 complexes are tabulated in Table 3. The interactions are classified in two categories: that the $E^{(2)}$ value is larger than 2 kcal/mol for strong hydrogen bond interaction and from 0.5 kcal/mol to 2kcal/mol for weak hydrogen bond interaction [30]. The interactions are detailed as follows: for the C1 complex, the highest interaction energy was observed for the lone pairs interaction LP (S 218) $_{2MMPT}$ →σ*(C 65 - H 70) $_{HPβ-CD}$, LP (S 219) $_{2MMPT}$ →σ*(O 133 - H 134) $_{HPβ-CD}$, LP (O22)$_{HPβ-CD}$ →σ*(N 220- H 234)$_{2MMPT}$ and LP (O194)$_{HPβ-CD}$→σ*(C 232 - H 241)$_{2MMPT}$, with stabilization energy ranged between 2.02 to 28.01 kcal /mol.

Table 3. NBO electronic transitions of the intermolecular HBs of host-guest inclusion complexes of 2MMPT with HPβ-CD for C1 and C2 complexes and the corresponding stabilization energies ($E^{(2)}$).

Donor	Acceptor	$E^{(2)}$ Bp86-D3/6-31G(d,p)	
		In gas phase	In aqueous phase
C1 complex			
LP (2) S 218	σ*(C 65 - H 70)	4.62	2.28
σ (C 26 - H 92)	σ*(C 228 - H 237)	0.25	0.58
σ (C 56 - H 97)	σ*(C 229 - H 238)	0.11	0.08
LP (2) S 219	σ*(O 133 - H 134)	28.01	20.61
σ (C 169 - H 171)	σ*(C 231 - H 240)	0.12	0.19
σ (C 225 - H 235)	σ*(O 135 - H 136)	0.08	0.17
σ (C 226 - H 236)	σ*(O 80 - H 81)	0.05	0.05
σ (C 227 - H 237)	σ*(C 26 - H 92)	0.21	0.91
σ (C 229 - H 238)	σ*(C 56 - H 97)	0.31	0.13
LP (1) O 22	σ*(N 220 - H 234)	2.02	6.23
LP (2) O 194	σ*(C 232 - H 241)	3.10	4.96
σ (C 231 - H 240)	σ*(C 169 - H 171)	0.10	0.30
σ (C 232 - H 241)	σ*(O 194 - H 195)	0.20	0.06
C2 complex			
σ (C 25 - H 30)	σ*(N 220 - H 234)	0.07	0.21
σ (C 35 - H 40)	σ*(N 220 - H 234)	0.10	0.08
σ (C 39 - H 121)	σ*(C 228 - H 237)	0.12	0.12
σ (C 66 - H 71)	σ*(C 230 - H 239)	0.28	0.23
σ (C 225 - H 235)	σ*(C 35 - H 40)	1.06	0.83
LP (2) S 218	σ*(O 125 - H 126)	8.38	7.67
σ (C 226 - H 236)	σ*(C 6 - H 9)	0.60	0.19
LP (1) O 73	σ*(C 226 - H 236)	2.01	2.09
σ (C 227 - H 230)	σ*(O 183 - H 184)	0.17	0.10
LP (2) O 121	σ*(N 220 - H 234)	6.44	6.15
σ (C 228 - H 237)	σ*(O 121 - H 122)	0.43	0.35
σ (C 230 - H 239)	σ*(C 5 - H 8)	0.24	0.06
σ (C 231 - H 232)	σ*(O 133- H 134)	0.17	0.09
σ (C 233 - H 243)	σ*(C 163 - H 164)	0.18	0.06

For the C2 complex, donor–acceptor interactions are observed between LP (O121) $_{HP\beta\text{-}CD}\rightarrow\sigma^*$(N 220 - H 234) $_{2MMPT}$, LP (S218) $_{2MMPT}\rightarrow\sigma^*$(O 125 - H 126) $_{HP\beta\text{-}CD}$ and LP (O 73)$_{HP\beta\text{-}CD}\rightarrow\sigma^*$(C 226 - H 236)$_{2MMPT}$ with stabilization energy ranged between 2.09 to 8.38 kcal/mol. Thus, we concluded that the higher $E^{(2)}$ energy for the C1 complex indicates a greater interaction compared to the C2 complex. This result is in agreement with the binding and interaction energies of the C1 complex. The interactions described above are hydrogen bonds. The other types of orbital's interactions: σ→σ* are relatively low, in which their stabilization energies vary between 0.05 and 1.06 kcal/mol. These interactions are classified as weak hydrogen bonds. From this NBO analysis, it can be concluded that these complexes are stabilized by strong hydrogen bonds and van der Waals interactions.

Energy decomposition analysis

The generated structures optimized by the PM3 method at each step from −6 to +6 Å were analyzed by EDA at BP86-D3/6-31G (d,p) functional. The computed results are depicted in Fig. 9 and in Table 6S in supporting information. The total binding energies are the summation of four terms, *viz*., Pauli repulsion (ΔE^{Pauli}), electrostatic (ΔE^{elstat}), orbital (ΔE^{orb}) and dispersion (ΔE^{disp}) terms. In the EDA analysis, the 2MMPT is considered as one fragment and the HPβ-CD is considered as the other fragment. From Table 6S and Fig. 9 it can be seen that the repulsive term, ΔE^{Pauli}, is positive in value and is responsible for steric repulsion [31, 32]. The term ΔE^{Pauli} provides the repulsive interaction between the occupied orbitals of two interacting fragments. The maximum contribution at each step comes from ΔE^{elstat} and plays a major role in stabilizing the two complexes. The non-covalent term ($\Delta E^{elstat} + \Delta Ed^{isp}$) contributes more largely in the total stabilization

than the covalent term (ΔE^{orb}) confirming the non-covalent nature of the interactions between host and guest. From the EDA results, we can conclude that in the attractive forces, the electrostatic interaction dominates in the intermolecular bonding between the HPβ-CD and the 2MMPT.

QTAIM analysis

The intermolecular interactions in C1 and C2 complexes were further discussed through topological QTAIM analysis. Bader [33, 34] developed QTAIM quantum theory. It is based on the study of the topology of the electronic density, which characterizes the distribution of electrons in space.

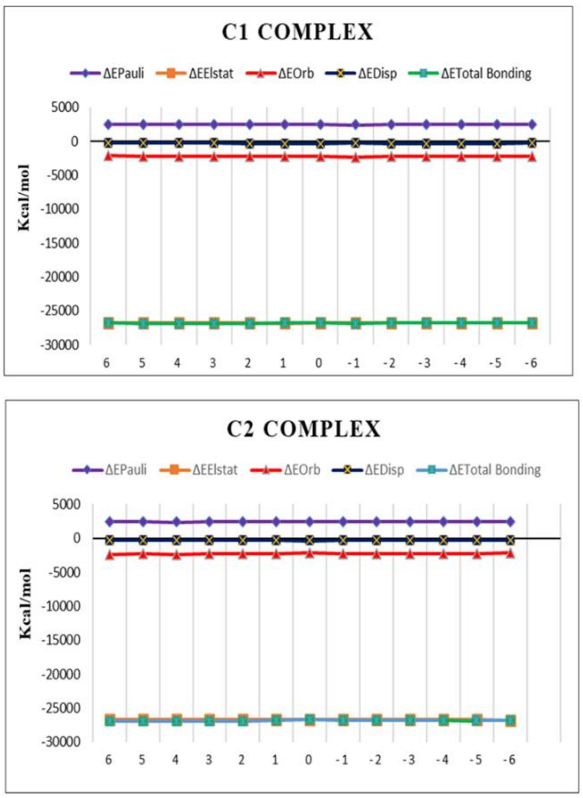

Fig. 9. Energy profiles of the generated structures at each step for C1 and C2 complexes obtained from the EDA analysis at BP86-D3/6-31G (d,p) level of theory.

It is allowed to determine the different characteristics that present the intra- and intermolecular interactions, precisely to find hydrogen bond strengths from different topological properties [35]. The Laplacian, local kinetic energy density G(r), local potential energy density V(r), and local electron energy density H(r) at the BCP are used to summarize the nature of the bond or interaction. According to QTAIM theory, a bond is characterized by the existence of a critical point of binding (BCP) [36]. The molecular graphs obtained for the studied inclusion complexes are given in Fig. 10. The different intermolecular interactions that exist in both complexes are shown in dotted lines.

The computed topological parameters corresponding to the intermolecular interactions of the two complexes such as electron densities (ρ), Laplacian of electron density ($\nabla^2(\rho)$), local kinetic energy density G(r), local potential energy density V(r), Hamiltonian kinetic energy H(r), -G(r)/V(r) ratio, electron localization function (ELF), localized orbital locator (LOL) and bond energies at the intermolecular bonding BCPs are listed in Table 4.

From Table 4 we observe that the obtained electron density and the Laplacian at the intermolecular BCPs are all positive for both complexes, showing the non-covalent nature of intermolecular bonding. Based on the Rozas *et al.* [37] criterion, the hydrogen bonds are classified as follows:

− Weak hydrogen bonds: $\nabla^2\rho$ (r) > 0 and H(rBCP) > 0;

− Moderate hydrogen bonds: $\nabla^2\rho(r) > 0$ and H(rBCP) < 0;

− Strong or very strong hydrogen bonds: $\nabla^2\rho(r) <$ 0 and H(r) < 0.

For all BCPs, $\nabla^2\rho(r) > 0$, H (r) > 0 and the interaction energies E_{HB} do not exceed 10 kcal/mol.

Based on the above topological and energetic results, one may conclude that the intermolecular interactions in the C1 and C2 complexes are weak and approve the electrostatic behavior of these interactions [38]. In addition, the ratio of -G(r)/V(r) is > 1, supporting the existence of weak intermolecular bonding between host and guest in the two complexes [39]. Additionally, a small value of ELF and LOL confirms the electrostatic nature of the interactions between host and guest molecules, which shows that electrons are not greatly localized at the BCPs.

The important advantage of the QTAIM application lies with the development of models correlating between the electron density $\rho_{(BCP)}$ and the interatomic distance. It has been found that the BCP is typically an excellent descriptor of the strength of the interactions; that is larger for shorter interatomic distances [40]. The plots of the electron density as a function of interatomic distances for C1 and C2 complexes are shown in Fig. 11. It can be seen that the dependence between the electron density and the hydrogen bond distances follows an exponential trend.

Table 4. Topological parameters obtained from QTAIM analysis for C1 and C2 complexes. The following topological parameters are given: the corresponding $d_{H\cdots X}$ distances; the electron density at BCP ρ(r), its Laplacian ∇2 (ρ), the kinetic electron energy density G(r) and the potential electron energy density V(r). All ρ(r), ∇^2 (ρ), G(r) and V(r) values in atomic units; E_{HB} in kcal/mol; bond length in Å.

	$d_{H\cdots X}$	ρ(r)	∇^2 (ρ)	G(r)	V(r)	H(r)	-G/V	LOL	ELF	E_{HB}
C1 complex										
N220-H234···O22	2.10	0.0189	0.0189	0.0218	-0.0206	0.0011	1.0583	0.1498	0.03010	6.46
C233-H244···O135	2.43	0.0089	0.0488	0.0095	-0.0068	0.0027	1.3971	0.1032	0.0130	2.13
C225-H235···O135	2.50	0.0082	0.0433	0.0082	-0.0056	0.0026	1.4643	0.1037	0.0132	1.76
C2 complex										
N220-H234···O121	2.15	0.0167	1.8	0.0189	-0.0171	0.0018	1.1053	0.1415	0.0264	5.37
C233-H244···O96	2.66	0.0052	2.9	0.0058	-0.0036	0.0022	1.6111	0.0726	0.0061	1.13
C228-H237….O121	2.50	0.0078	0.0455	0.0086	-0.0058	0.0028	1.4810	0.0937	0.0105	1.82

Fig. 10. Molecular topography analysis obtained from the AIM analysis of C1 and C2 complexes in aqueous phase at BP86-D3/6-31G (d,p) level of theory.

The corresponding relationships are given in Fig. 11. Excellent correlation is seen between $\rho_{(BCP)}$ and the hydrogen bond distances. Also, QTAIM characteristics are further described through hydrogen bond energies (E_{HB}) at the intermolecular BCPs estimated by using Espinosa equation [41] (see Table 4) and the kinetic electron energy density (G(r)). Fig. 12 displays E_{HB} as a function of the kinetic electron energy density (G(r)) showing a linear dependence. corresponding linear regression equations for C1 and C2 complexes are as follows:

E_{HB} = 555.28 G(r)-1.8111,
E_{HB} = 528.37 G(r)-1.4315.

An excellent linear correlation (R^2 = 0.9998 and 0.9972, respectively.for C1 and C2 complexes) is obtained between the hydrogen bond energies and the kinetic electron energy density (G(r)).

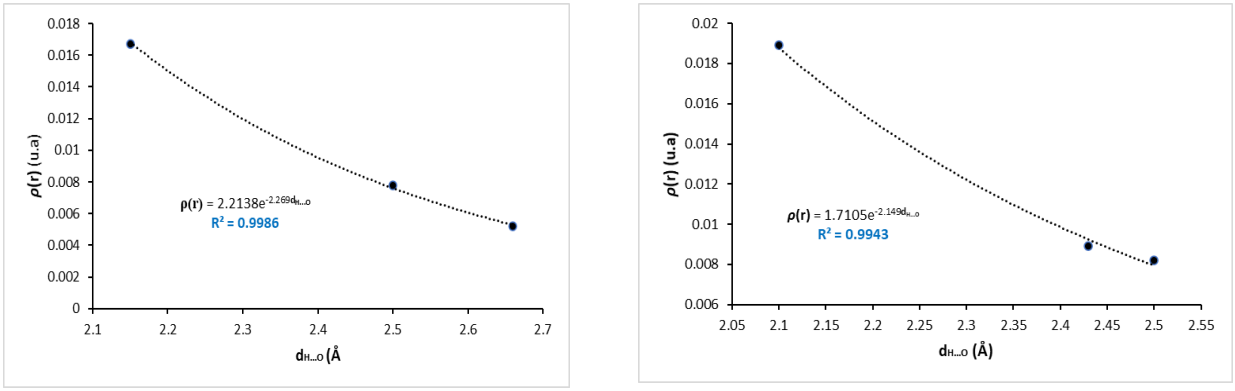

C1 complex C2 complex

Fig. 11. Electron densities (in au) as a function of the hydrogen bond distances (in Å) for C1 and C2 complexes.

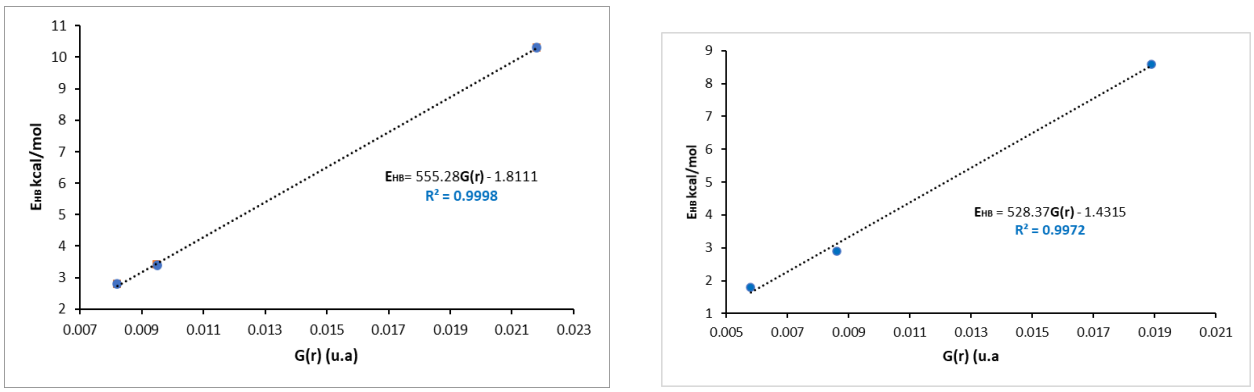

C1 complex C2 complex

Fig. 12. E_{HB} (in kcal/mol) as a function of kinetic electron energy density (G(r) (in au) for C1 and C2 complexes.

Non-covalent interactions-reduced density gradient analysis

NCI-RDG analysis presents a graphical visualization of the region where non-covalent interactions occur in real-space, and is capable of distinguishing hydrogen bonds, van der Waals interactions and repulsive steric interactions through simple color codes [42]. NCI is expressed in terms of the electron density, its Laplacian, and the reduced gradient of density. According to NCI analysis, the interaction types are determined by examination of the sign of the second eigenvalue λ_2. The strength and nature of interactions can be interpreted by the product sign λ_2 times ρ as given by RDG iso surfaces. (Sign λ_2) $\rho < 0$ for attractive interaction, (sign λ_2) $\rho > 0$ for a repulsive interaction, whereas the weak van der Waals types reveal (sign λ_2) $\rho \approx 0$ which are designed in the RDG isosurface with blue, red and green color, respectively [43]. Blue, green, and red color codes are used to describe stabilizing H-bonding, van der Waals, and destabilizing steric interaction, respectively [38]. The NCI plots for the two complexes are depicted in Fig. 13. The red areas observed indicate a steric repulsion and are localized mostly in the middle of the benzene rings and near the oxygens of carbonyl groups of HPβ-CD. The green areas observed between host and guest molecules indicate the existence of van der Waals and electrostatic interactions.

CONCLUSION

We applied a dispersion corrected density functional methodology to study non-covalent intermoleular interactions leading to the complex formation of 2MMPT with HPβ-CD. The calculated binding and interaction energies are in favor of the C1 complex where the guest molecule is totally encapsulated in the HPβ-CD cavity. Our theoretical ^{1}H NMR chemical shift results are in good agreement with the experimental data. The results of NBO analysis show that C1 and C2 were stabilized by weak and strong hydrogen bonds. Energy decomposition analysis indicated that the electrostatic interaction dominated among the attractive interactions in both complexes.

From the AIM results, one can conclude that the obtained electron density and the Laplacian at the

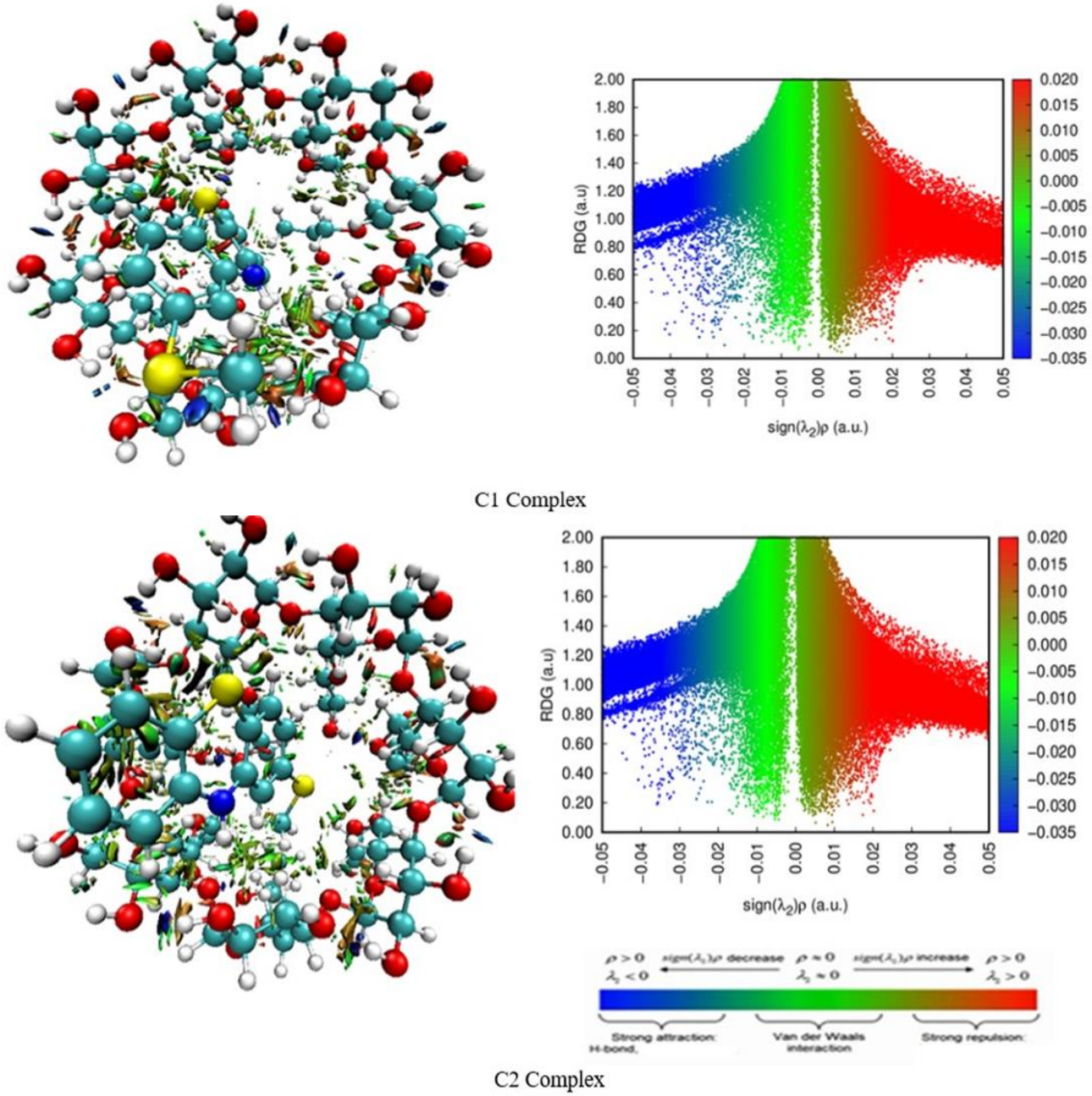

Fig. 13. Plots of RDG(s) *versus* the electron density multiplied by the sign of the second Hessian eigenvalue (sign λ2) ρ and the corresponding H-bond interaction for both complexes

intermolecular BCPs were all positive for both complexes, showing the non-covalent nature of intermolecular bonding. Finally, the NCI analysis shows that the van der Waals interactions and hydrogen bonds are the driving forces in stabilizing the complexes.

Acknowledgement: *The Algerian Ministry of Higher Education and Scientific Research supported the investigation.*

Conflict of interest: *The authors declare no conflict of interest.*

Supplementary Data File

REFERENCES

1. P. Sua, Z. Chena, W. Wu, *J. Chem. Phys. Lett*., **635**, 250 (2015).
2. R. F. W. Bader, *J. Chem. Rev*., **91**, 893 (1991).
3. F. Fuster, S. J Grabowski, *J. Phys. Chem.* A, **115**, 10078 (2011).
4. C. R. Landis, F. Weinhold, Discovering chemistry with natural bond orbitals, John Wiley& sons, 2012.
5. T. R. Ragia, K. Sivakumar, *J. Mater. Tod. Proc*., **14**, 395 (2019).
6. M. Krstic, S. P. Sovilj, S. Grguric-Sipka, I. Radosavljevic Evans, S. Borozan, J. F. Santibanez, J. Kocic, *Eur. J. Med. Chem*., **45**, 3669 (2010)
7. A. Lutka, B. Golda, *Acta Pol. Pharm*., **63**, 3 (2006).

8. Y. Fu, L. Liu, Q. X. Guo, *J. Phen. Macro. Chem*., **43**, 223 (2002).
9. M. E. Davis, M. E. Brewster, *Nat. Rev. Drug. Discov*., **31**, 1023 (2004).
10. L. Wang, J. Yan, L. Li, K. Xu, S. Li, P. Tang, H. Li, *J. Pharm. Biomed. Anal*., **117**, 453 (2016).
11. T. R. Ragia, K. Sivakumar, *Mater. Tod. Process*., **14**, 395(2019).
12. S. Grimme, J. Antony, S. Ehrlich, H. Krieg, *J. Chem. Phys*.,**132**, 154104 (2010).
13. S. Grimme, *J. Comput. Chem*., **27**, 1787 (2006).
14. S. Grimme, *J. Wires. Comput. Mol. Sci.*, **1**, 211 (2011).
15. H. Bouchemela, F. Madi, L. Nouar, *J. Inclus. Pheno. Macro. Chem*., **25**, 247 (2019).
16. S. Himri, I. Lafifi, A. Guendouzi, M. Cheriet, L. Nouar, F. Madi, *J. Mol. Liq*., **280**, 218 (2019).
17. P. L. Verma, S. P. Gejji, *J. Mol. Liq.*, **293**, 111548 (2019).
18. M. J. Frisch, G. W. Trucks, B. Schlegel, G. E. Scuseria, M. A. Robb, J. R. Cheeseman et al., Gaussian 09, revision A.01, 2013.
19. T. Lu, Chen, F. Multiwfn, *J. Comput. Chem*., **33**, 580 (2011).
20. W. Humphrey, A. Dalke, K. Schulten, *J. Mol. Graph*., **14**, 33 (1996)
21. ADF2017, SCM, Theoretical Chemistry, Vrije Universiteit, Amsterdam, The Netherlands, http://www.scm.com.
22. K. Fukui, *J. World.Scientific*, **150-170** (1997) (1981-1990).
23. F. De Proft, J. M. Martin, P. Geerlings, *J. Chem. Phys. Lett*.,**256**, 400 (1996).
24. R. R. Contreras, P. Fuentealba, M. Galván, P. Pérez, *J. Chem. Phys. Lett.*, **304**, 405 (1999).
25. R. Arora, U. Issar, R. Kakkar, *J. Comput. Theor. Chem*., **1138**, 5765 (2018).
26. D. N. Lande, S. A. Bhadane, S. P. Gejji, *J. Phys. Chem*., A, **121**, 1814 (2017).
27. M. Snehalatha, C. Ravikumar, I. H. Joe, N. Sekar, V. S. Jayakumar, *Spectrochim. Acta* A, **72**, 646 (2009).
28. C. James, A. A. Raj, R. Reghunathan, V. S. Jayakumar, I. H. Joe, *J. Spectrosc. J. Raman. Spectrom.*, **37**, 1381 (2006).
29. H. Ghalla, N. Issaouia, F. Bardak, A. Atac, *Computational Materials Science*, **149**, 291 (2018).
30. G. Uccello-Barretta, F. Balzano, G. Sicoli, C. Fríglola, I. Aldana, A. Monge, D. Paolino, S. Guccione, *Bioorg. Med. Chem*., **12**, 447 (2004).
31. T. Ziegler, A. Rauk, *Theor. Chim. Acta* **46**, 1 (1977).
32. N. S. Venkataramanan, A. Suvitha, Y. Kawazoe, *J. Mol. Liq.*, **260**, 1829 (2018).
33. R. F. W. Bader, M. A. Austen, *J. Chem. Phys*., **107**, 427 (1997).
34. R. F. W. Bader, Atoms in molecules: A. Quantum theory, Oxford Univ. Press, 1990, p. 12.
35. S. Gatfaoui, N. Issaoui, T. Roisnel, H. Marouani, *Journal of Molecular Structure*, **1191**, 183 (2019).
36. O. Noureddine, S. Gatfaoui, S. A. Brandan, A. Sagaama, H. Marouani, N. Issaoui, *Journal of Molecular Structure*, **1207**, 127762 (2020).
37. I. Rozas, I. Alkorta, J. Elguero, *J. Am. Chem. Soc*., **122**, 11154 (2000).
38. M. Tahenti, S. Gatfaoui, N. Issaoui, T. Roisnel, H. Marouani, *Journal of Molecular Structure*, (2020), doi: https://doi.org/10.1016/.
39. N. S. Venkataramanan, A. Suvitha, Y. Kawazoe, *J. Mol. Graph. Model.*, **78**, 48 (2017).
40. S. J. Grabowski, W. Andrzej Sokalski, J. Leszczynskin, *Chem. Phys*., **337**, 68 (2007).
41. E. Espinosa, E. Molins, C. Lecomte, *J. Chem. Phys. Lett.*, **285**, 170 (1998).
42. E. R. Johnson, S. Keinan, P. Mori-Sánchez, J. Contreras-García, A. J. Cohen, W. Yang, *J. Am. Chem. Soc*., **132,** 6498 (2010).
43. G. Saleh, C. Gatti, L. Lo Presti, J. Contreras-Garcia, *J. Chem*., **18**, 15523 (2012).